ACS APPLIED MATERIALS & INTERFACES

Research Article

www.acsami.org

Tuning the Magneto-optical Response of Iron Oxide Nanocrystals in Au- and Ag-Based Plasmonic Media

M. Caminale,[†,¶] L. Anghinolfi,[†,⊥] E. Magnano,[‡] F. Bondino,[‡] M. Canepa,[§,†] L. Mattera,[§,†] and F. Bisio*[,¶]

[†]Dipartimento di Fisica, Università di Genova, via Dodecaneso 33, I-16146 Genova, Italy

[‡]IOM-CNR, Laboratorio Nazionale TASC, Strada Statale 14, km 163.5, Basovizza, I-34149 Trieste, Italy

[§]CNISM, Sede Consorziata di Genova, via Dodecaneso 33, I-16146 Genova, Italy

[¶]CNR-SPIN, C.so Perrone 24, I-16152 Genova, Italy

Supporting Information

ABSTRACT: We investigated the magneto-optical response of chemically synthesized iron oxide magnetic nanocrystals, optically coupled with ordered planar arrays of plasmonic nanoparticles. We compare the signals from two classes of systems, featuring either Au or Ag as the plasmonic counterpart. The localized surface plasmon resonance of the Ag and Au nanoparticles arrays were superimposed or detuned, respectively, with respect to the dominant magneto-optical transitions of the magnetic material. Under resonance, a significant enhancement of the magneto-optical signal was observed. In both cases, we could separate the purely plasmonic and the magnetic contributions in the magneto-optical spectrum of the optically coupled composite based on their different magnetic-field dependence.

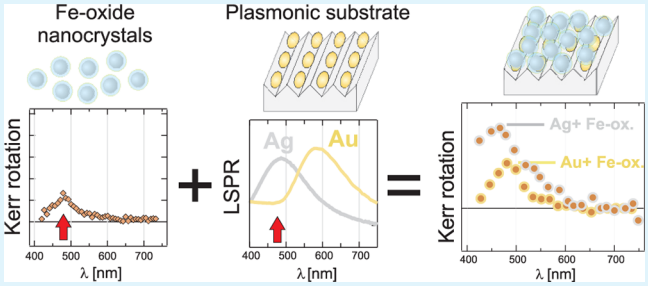

KEYWORDS: *magnetic nanoparticles, maghemite, plasmonics, magneto-optics, gold, silver*

INTRODUCTION

In correspondence of the localized surface plasmon resonance (LSPR) of noble-metal nanoparticles (NPs),[1−5] the local electromagnetic (EM) field in the near vicinity of the NP surface can be very strongly enhanced with respect to its free-space value.[4] If optically active materials are appropriately placed within the field-enhancement region, their optical response can be strongly affected by the local field. An interesting application of this effect consists of modifying the magneto-optical (MO) response of magnetic materials via the plasmon-enhanced EM fields.[6−20] The coupling of plasmonic and magnetic materials, or the plasmonic excitation of magnetic nanostructures,[19,21] form the basis of interesting phenomena such as the LSPR-induced enhancement of the MO response,[6−16,19,20] and find application in, e.g., the plasmon-mediated heat-assisted magnetic recording.[17,18]

The enhancement of the MO response in magnetoplasmonic systems is directly correlated with the EM field intensity within the MO-active material, thus making this effect strongly sensitive to the degree of optical coupling between the plasmonic and the magnetic counterparts.[11,22] Provided that the spatial-proximity condition between the two materials is met,[22] the general requirement for maximizing the LSPR-enhancement effect is tuning the LSPR with the dielectric—more specifically, the MO—response of the magnetic substance.[23] For transition metals, characterized by relatively smooth optical response and broadband MO spectra,[24,25] the LSPR matching is not an issue,[11,14,16,26] while transition-metal oxides and other compounds[27−30] can be less straightforward, from this point of view.[7,9] Tuning the LSPR with the intrinsic excitations of the magnetic counterpart can also shed further light on the mechanism of plasmon-induced MO enhancement, helping maximize the MO enhancement in optically coupled magnetoplasmonic heterostructures. For this purpose, independently tuning the plasmonic and magnetic materials' properties prior to their merging is clearly an advantage.

In this article, we address the MO response of two-dimensional (2D) layers of iron oxide nanocrystals (NC) optically coupled with plasmonic substrates composed of ordered 2D arrays of noble-metal nanoparticles. Plasmonic arrays composed of Ag NPs, whose LSPR is spectrally superimposed with the dominant MO transitions of iron oxide, yield significant enhancements of the iron-oxide MO signal. Replacing Ag with Au, whose LSPR is spectrally detuned with respect to the NC MO transitions, strongly lowers their MO response. The comparison of the two systems' response thus pinpoints the role of the LSPR-MO spectral matching on the plasmon-induced enhancement. In both cases, we also observed that the contribution to the MO signal arising from the magnetic and the plasmonic counterparts can be clearly

Received: November 15, 2012
Accepted: March 4, 2013
Published: March 4, 2013

separated, even under optical coupling, based on their markedly different magnetic-field dependence.

EXPERIMENTAL SECTION

Fabrication of the Plasmonic Substrates. The samples consisted of planar, 2D arrays of metallic nanoparticles (Au or Ag) supported on an insulator substrate, on top of which iron oxide NCs are deposited by dip-and-dry procedures.

The 2D arrays of plasmonic NPs were fabricated by depositing the noble metals onto the self-organized nanometric uniaxial triangular-wave pattern that spontaneously develops on the LiF(110) surface following homoepitaxial growth.[31,32] Optical-quality LiF(110) substrates (Crystec GmbH) were employed. Approximately 240 nm of LiF were deposited at a substrate temperature of T = 620 K to achieve the formation of the LiF nanostructures. Noble metals (Ag, 99.999% purity (Mateck GmbH) and Au, 99.99% purity (Mateck GmbH)) were deposited in high vacuum ($p < 5 \times 10^{-8}$ mbar) by molecular beam epitaxy at room temperature at a 60° angle of incidence, with respect to the surface normal. The equivalent deposited thickness was ~3 nm for Ag and ~5 nm for Au. The metal/LiF systems were then flashed at T = 670 K.[33]

The atomic force microscopy (AFM) characterization was performed by means of a Multimode/Nanoscope IV system (Digital Instruments-Veeco). For quantitative analysis purposes, the NPs observed in the images were discriminated and isolated by means of threshold algorithms. The in-plane aspects of the isolated NPs were fitted as ellipses, and the mean in-plane NP size and the relative distances between the NP centers could be deduced.

Synthesis of Iron Oxide Nanocrystal. The Fe_3O_4 NCs coated with oleic acid were prepared via thermal decomposition of the iron(III)-oleate complex in 1-octadecene in the presence of oleic acid in a 3:1 relationship, with respect to the metal complex. The solution was slowly heated under a nitrogen atmosphere to 312 °C and then aged at that temperature for 240 min, generating the iron oxide NCs.[34,35] The NCs, as observed via TEM, exhibit a cubic shape and a very narrow distribution of their mean core diameter (d_{core} = 13 ± 1.3 nm).[36,37] When dispersed in hexane, the hydrodynamic diameter d_{hydro} of the iron oxide NCs obtained from dynamic light scattering (DLS) was monodisperse, d_{hydro} = 16 ± 4 nm. The NC showed negligible tendency to aggregate in suspension. For the NC deposition, the substrates were immersed in the NC hexane suspension with a Fe concentration of ~6 μg/mL for 5 min, then rinsed in pure hexane and dried under nitrogen flux.

Optical and Magneto-optical Characterization. The reflectivity measurements were performed in the experimental geometry depicted in the top part of Figure 2 (shown later in this work): the angle of incidence was θ = 50° and light polarization perpendicular to the LiF ridges, determined using a J. A. Woollam Model M-2000X variable-angle ellipsometer/reflectometer.

The calculation of the optical reflectivity of the NP/LiF systems was performed according to the model described in ref 33, keeping into account the EM interactions between the NPs and between the NPs and the substrate. The NPs were modeled as being immersed in a thin effective-medium layer with a dielectric constant equal to the average dielectric constants of the vacuum and the substrate. The NP array morphology was fed to the model from the AFM images. The presence of the NCs onto the NP/LiF system was simulated by appropriately augmenting the dielectric constant of the medium surrounding the NPs, and increasing the effective-medium layer thickness by a quantity d_{hydro}, as specified in detail in ref 37. The optical constants of maghemite were used for the NCs.[38]

The MO response was assessed by the polar magneto-optical Kerr effect (MOKE), in the same optical geometry as reflectivity. The sample was illuminated with an *s*-polarized white beam from a xenon lamp (Figure 3, top right, shown later in this work). The reflected beam was analyzed by a linear polarizer detuned by an angle α from the extinction condition, and fed to a spectrometer with a wavelength range of λ = 400−1000 nm (Ocean Optics, Model USB-2000). The intensity spectra for *opposite directions of an external field*, H = ±5000 Oe, applied normal to the sample surface, were recorded for a set of analyzer angles in the $-1.5° < \alpha < 1.5°$ interval. The intensity as a function of α and λ for each field orientation was fitted against a cosine-square dependence, allowing one to deduce the wavelength dependence of the purely magnetization-induced rotation, the Kerr angle ($\phi_K(\lambda)$). Hysteresis loops of the samples at all λ could be measured in parallel by setting the analyzer at a fixed angle α^* (typically chosen to maximize the magnetic contrast) and recording the light intensity after the analyzer while sweeping the external field **H**.

RESULTS AND DISCUSSION

In Figures 1a and 1b, representative AFM images of the 2D arrays of Ag/LiF and Au/LiF are shown. The NPs are fairly regular in size and relative position in both cases. Notably, their arrangement exhibits a characteristic uniaxial alignment induced by the triangular-wave pattern of the underlying substrate, and the Au NPs are slightly elongated along the ripple direction.[33] In the insets of Figures 1a and 1b, the 2D distribution of the

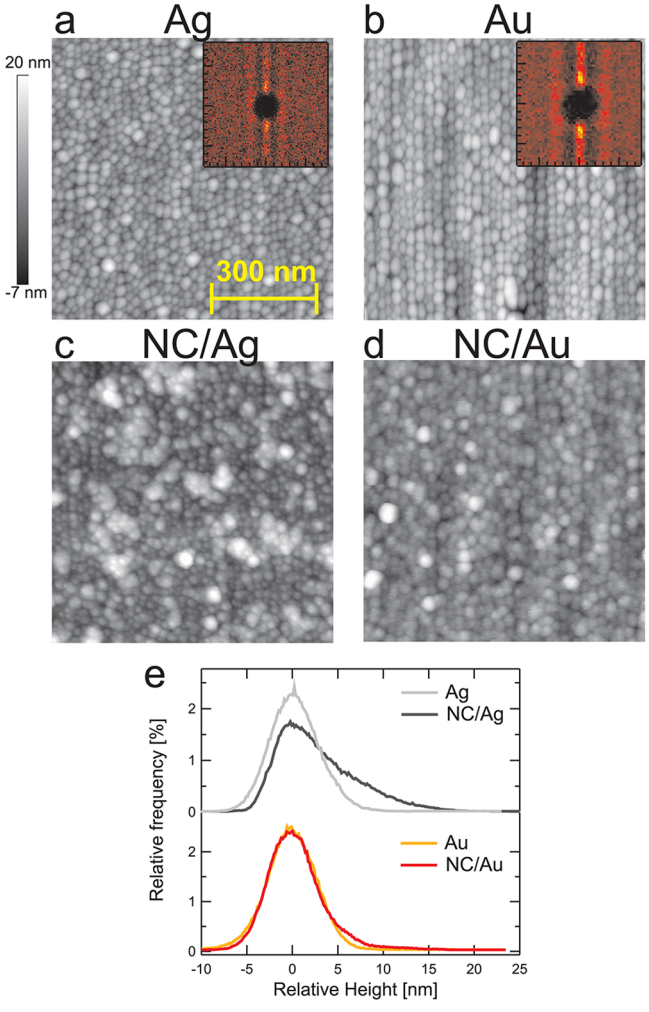

Figure 1. (a, b) AFM images of the Ag/LiF and Au/LiF plasmonic substrates prior to the NC deposition (the height scale reported in panel a is valid for all images, and all images have the same size (800 nm × 800 nm)); insets of panels a and b show two-dimensional (2D) distributions of the nanoparticle (NP) center-to-center distances extracted from the AFM images (inset size: 80 nm × 80 nm). (c, d) AFM images of the Ag/LiF and Au/LiF systems following the NC deposition. (e) Histograms of the height distributions, relative to the AFM images.

dx.doi.org/10.1021/am3027234 | ACS Appl. Mater. Interfaces 2013, 5, 1955−1960

NP center-to-center distances deduced from the AFM images are reported. The uniaxial symmetry of the NP arrangement is apparent. In the bottom graph, the height histograms of the images are reported. Both histograms have a Gaussian shape, with a full width at half maximum (fwhm) of 7.5 and 7.4 nm for Au and Ag, respectively, arising from the root-mean-square (rms) surface roughness of the samples. AFM-tip effects were not considered.

In Figures 1c and 1d, we report two AFM images of the Ag and Au arrays following the deposition of the magnetic NCs. In both cases, a clear difference can be seen following the NC deposition, as an increased disorder in the pattern. Overall, however, the NC patterns have preserved a certain degree of the characteristic uniaxial symmetry of the noble-metal NP arrays, somehow suggesting the formation of a relatively thin NC layer on top of the plasmonic substrate.

The LSPR excitation of the plasmonic arrays is manifested as a marked peak in their *s*-polarized reflectivity spectra (R_s).[33] The bare Ag/LiF sample exhibits its LSPR peak at $\lambda \approx 473$ nm (Figure 2, left panel, red markers),[39] while Au, because of its

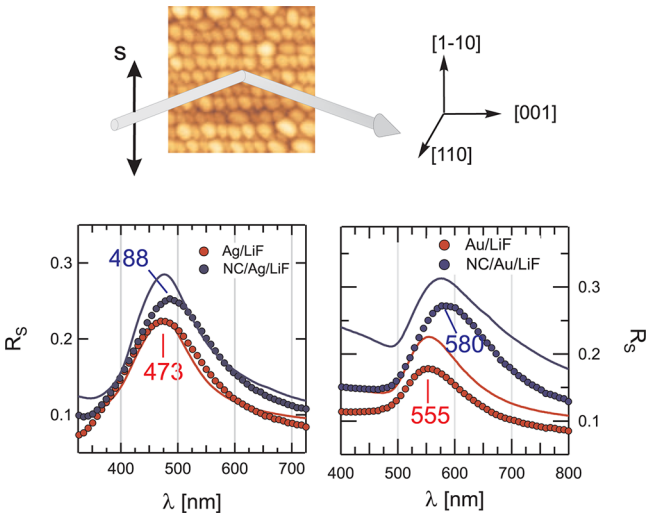

Figure 2. Top panel shows the experimental geometry for the reflectivity measurements: the angle of incidence was $\theta = 50°$, with respect to the surface normal, and the light was polarized transverse to the LiF nanoridges. Bottom panels show experimental *s*-polarized reflectivity spectra of the Ag sample (left) and the Au sample (right) before and after the NC deposition (red and blue markers, respectively). The corresponding calculated spectra are reported as the red and blue lines, respectively.

different dielectric function, has its LSPR red-shifted to $\lambda \approx 555$ nm (Figure 2, right panel, red markers). Following the deposition of the NCs, the LSPR peaks red-shift, by ~15 nm for Ag and ~25 nm for Au (blue markers). Qualitatively, the LSPR redshift is consistent with the increase of the dielectric constant of the noble-metal NP environment due to the NCs.[3] The LSPR shift confirms the close physical proximity between the plasmonic particles and the NCs and their mutual optical coupling.

The $\phi_K(\lambda)$ spectrum of NC/Ag is reported as the black line in Figure 3a. The spectrum can be readily compared with the reference MO response of the NCs deposited on a *flat* Al surface, reported as the gray diamonds in the figure. Aluminum indeed provides a flat optical response and a negligible MO background, adding no substrate contribution. The NC/Ag

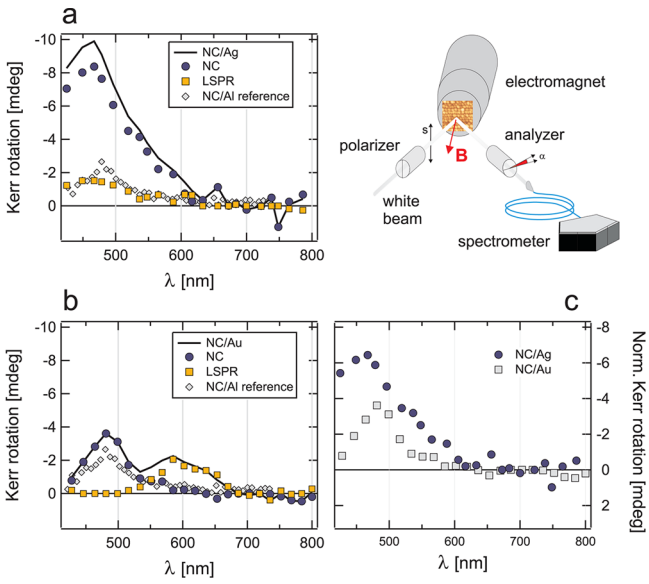

Figure 3. (a) Magneto-optical Kerr effect (MOKE) spectrum $\phi_K(\lambda)$ of the NC/Ag/LiF system (black line), NC contribution (blue circles), LSPR contribution (orange squares), NC/Al reference spectrum (gray diamonds) (left) and experimental geometry for the MOKE measurements (right). (b) MOKE spectrum $\phi_K(\lambda)$ of the NC/Au/LiF system (black line), NC contribution (blue circles), LSPR contribution (orange squares), and NC/Al reference spectrum (gray diamonds). (c) NC contribution to the MOKE spectra of NC/AG/LiF (blue circles) and NC/Au/LiF (gray squares) normalized to their NC coverage.

MO response is very similar in shape to the reference spectrum, since both consist of a single, broad peak with a maximum near $\lambda = 470–480$ nm. However, the NC/Ag Kerr rotation is much larger, with an almost 5-fold intensity increase at the maximum. We notice that, for Ag, the LSPR spectrally overlaps the MO peak of the reference NC/Al.

When we replace Ag as the plasmonic counterpart with Au, whose LSPR is detuned with respect to the NC MO peak, the MO response strongly changes. The ϕ_K spectrum of NC/Au (Figure 3b, black line) differs both in intensity and in shape, with respect to Ag. For Au, $\phi_K(\lambda)$ exhibits a double-peak structure, at $\lambda \approx 480$ nm and $\lambda \approx 580$ nm, and its peak intensity is much lower than Ag, very similar to the reference NC/Al at $\lambda \approx 480$ nm.

The differences in the spectra are interestingly mirrored by corresponding variations in the hysteresis loop shape between the two systems as a function of wavelength. Hysteresis loops at the selected wavelengths $\lambda = 480$ nm (corresponding to the maximum NC MO response and to the Ag LSPR), and $\lambda = 580$ nm (corresponding to the Au LSPR) are reported in Figure 4. At $\lambda = 480$ nm, the loops for NC/Ag and NC/Au (Figures 4a and 4b, red markers) both have a Langevin-like shape, while NC/Ag still shows a seemingly linear increase of the MOKE signal above $H \approx 3$ kOe, NC/Au seems to saturate beyond that value. At $\lambda = 580$ nm, the difference is striking: here, it is NC/Ag that exhibits a clear Langevin shape, whereas for NC/Au, the Kerr signal dependence on the applied magnetic field is linear.

The wavelength-dependent shape of the hysteresis loops stems from the uncorrelated superposition of the MO contributions of the plasmonic and the magnetic counterparts, each exhibiting a different magnetic-field dependence. The

dx.doi.org/10.1021/am3027234 | ACS Appl. Mater. Interfaces 2013, 5, 1955–1960

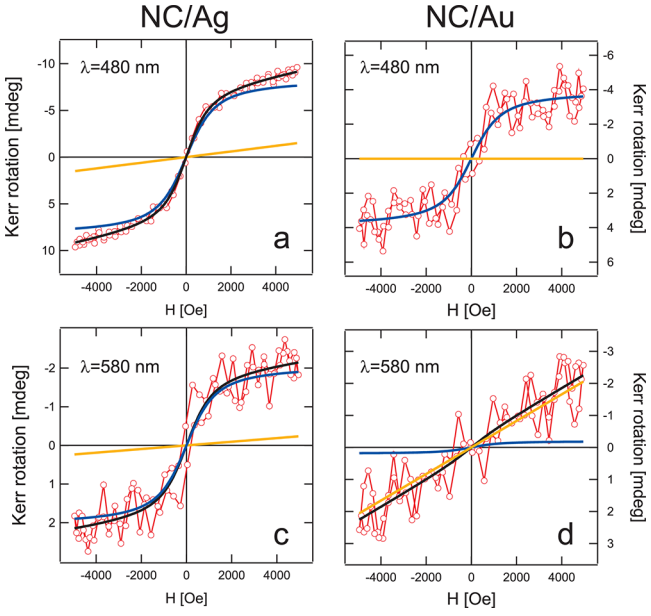

Figure 4. MOKE hysteresis loops recorded at λ = 480 nm ((a) NC/Ag and (b) NC/Au) (red symbols) and at λ = 580 nm ((c) NC/Ag and (d) NC/Au) (red symbols). The best fits to the hysteresis loops, the Langevin (NC) contribution, and the linear (LSPR) contribution are shown as the black, blue, and orange lines, respectively.

magnetization of the NC ensemble—and, hence their MO response—is indeed expected to follow a Langevin function, as a function of the applied field. The MO response of the plasmonic NPs, which is observable even in the presence of the NCs, instead has a linear dependence on H.[40−42]

In the $\phi_K(\lambda)$ spectra, the two contributions are inextricably superimposed. The relative weight of each contribution to the spectra can be instead derived from the hysteresis loops. In order to do this, we fitted each loop as the weighted sum of a Langevin function and a linear term. Such Langevin and linear terms yield the NC and plasmonic contributions to the overall spectra (see the Supporting Information for details about the fitting procedure). The magnetic-field dependence of each contribution is explicitly shown in the hysteresis loops of Figure 4. There, the blue, orange, and black lines represent the contribution of the NCs (Langevin), the NPs (linear), and their sum, respectively. The spectral dependence of the NC and the plasmonic contributions for NC/Ag and NC/Au is reported in Figures 3a and 3b, respectively, as blue circles (representing the NC contribution) and orange squares (representing the LSPR contribution). We notice that, since the loops allow to ascertain the relative weight of each contribution in the overall spectra, the sum of the NC and NP spectra, by definition, is equal to the overall ϕ_K spectra.

The plasmonic contribution to $\phi_K(\lambda)$ yields a single broad peak in the spectra, with ∼2 mdeg intensity, centered around 470 and 600 nm for NC/Ag and NC/Au, respectively (i.e., in correspondence of the systems' LSPR).[41] Instead, the NC contribution for NC/Au shows a peak at 480 nm, with a maximum of $\phi_K \approx 3.5$ mdeg, whereas for NC/Ag, the NC MO peak is slightly blue-shifted to $\lambda \approx 465$ nm and is significantly larger ($\phi_K \approx 8.5$ mdeg).

The most interesting aspect that emerges from the MO characterization of the Ag- and Au-based samples is the largely different MO response of their "magnetic" counterpart. Before discussing its origin, it is worth recalling that, in the Au- and Ag-based samples, the deposited NCs belonged to the same original suspension. In addition, it is necessary to quantify the amount of NCs deposited on each plasmonic substrate, in order to exclude MO enhancement because of different NC-layer thickness.

To this end, in Figure 2, we reported the calculated R_s spectra for the bare Ag/LiF and Au/LiF arrays (red lines) and those calculated in the hypothesis of a single NC layer deposited on the Ag/LiF and Au/LiF arrays (blue lines). The change in experimental reflectivity, following the NC deposition, is well-reproduced by the optical calculations, suggesting that the amount of NCs deposited on each plasmonic substrate was comparable to a single NC layer. In the Au case, the width of the height distribution deduced by AFM (hence, the sample roughness) has remained almost unchanged, following the NC deposition (see Figure 1e, red line), suggesting the formation of a compact NC layer: taking the optical data into account, it can be thus inferred that a single NC layer was deposited on Au/LiF. In the Ag sample, the height distribution (the dark-gray line in Figure 1e) exhibits a high-z tail, whose origin is easily traced to the presence of small agglomerates on top of a compact base layer. Assuming, based on the optical modeling, that such a base layer represents the first NC layer deposited on the Ag/LiF NPs, the integral of the high-z tail would account for a volume corresponding to 0.3 NC layers. Therefore, for this sample, the amount of deposited NCs can be estimated to be, at most, 1.3 monolayers. In Figure 3c, the NC contributions the Kerr spectra normalized to the so-obtained coverage are reported.

In both systems, the optical coupling between the plasmonic and magnetic counterparts has been achieved, as testified by the NC-induced LSPR shift. Therefore, the difference between the Ag and Au case should be ascribed to the different influence of the substrate's LSPR on the NC MO response, i.e., to the different spectral overlap between the LSPR and the characteristic MO transitions of the NCs.

The reference $\phi_K(\lambda)$ spectrum of NC/Al (gray diamonds in Figure 3) shows a marked peak at ∼480 nm,[9,30] and a fairly small signal in the red spectral range. Such a MO response suggests that the iron oxide NCs are mainly composed of maghemite (γ-Fe_2O_3),[9] produced upon oxidation of Fe_3O_4, a conclusion also supported by X-ray absorption spectroscopy data measured at the Fe $L_{2,3}$ edge, reported in the Supporting Information.[43] The dominant MO feature of the maghemite spectrum—the 480-nm peak—is due to a complex crystal field transition in the $3d^5$ orbital of Fe^{3+}, and has been identified as a general feature of compounds containing Fe^{3+}.[9,29] Weaker MO structures are present in γ-Fe_2O_3 at ∼530 nm.[9,29]

In the Ag case, for which a strong *spectral* overlap between the LSPR and the dominant NC MO transitions is present, the MO response of the NCs is much larger than the reference spectrum, clearly indicating that some form of MO enhancement has occurred. In comparison, when the LSPR is strongly detuned with respect to the major NC MO transitions, as in the Au case, the NC spectrum remains substantially unchanged with respect to the reference NC/Al data. According to the analysis reported in Figure 3b for Au, the LSPR has indeed no overlap with the 480-nm iron oxide peak, and only a weak superposition with the weaker structure at 530 nm. Instead, the LSPR sits in a range where the MO signal of the NCs alone is extremely weak. Thus, the 600 nm-peak of the Au $\phi_K(\lambda)$ has a purely "plasmonic" character, while the 480-nm peak is of

purely magnetic origin, although without sizable MO enhancement.

Although the use of two different substrates clearly affects the optical response via dielectric-constant effects, the behavior we observed does not fit with the dielectric enhancement,[7] in which a variation in the diagonal elements of the effective dielectric tensor outside the LSPR range accounts for most of the MO enhancement, since such enhancement, in our case, spectrally overlaps the LSPR. This points to the likely occurrence of a magnetoplasmonic ehnancement in the NC/Ag sample, achieved via spectrally matching the iron oxide dielectric properties with the LSPR in an optically coupled hybrid magnetic/plasmonic medium. However, the complex morphology of the self-organized plasmonic systems does not lend itself easily to the calculation of realistic near-field distribution maps, thus preventing the establishment of a direct correlation between the MO enhancement and the field-enhancement value on each sample.

In addition to the different degree of enhancement observed in Au- and Ag-based systems, we also note that, in the samples, it is possible to separately assess the purely plasmonic contributions and the magnetic contributions to the overall MO signal also in the presence of optical coupling, in analogy with that reported in ref 42. This phenomenon is apparent in the λ-dependent hysteresis loops, where the responses of the two materials are distinguishable upon appropriate data analysis. From the point of view of data interpretation, disentangling the two contributions represents an excellent aid to correctly assess the mechanisms underlying the formation of the collective MO response of composite materials. In this framework, therefore, a more-extended use of this procedure in magnetoplasmonic could bring significant advantages in the field.

CONCLUSIONS

We have reported the magneto-optical (MO) response of hybrid nanostructured media consisting of optically coupled magnetic nanocrystals and plasmonic nanoparticles two-dimensional (2D) arrays, comparing the MO response of two classes of samples, similar by design but featuring either Au or Ag as the plasmonic counterpart. The choice of either Ag or Au as the plasmonic material allows one to spectrally tune or detune the LSPR, with respect to the dominant MO transitions of the magnetic NCs, thereby allowing to either achieve or not a plasmon-enhanced MO response in the NCs.

We further showed the possibility of disentangling the plasmonic and magnetic contributions to the overall magneto-optical signal based on their different magnetic field dependence, opening the possibility of directly monitoring the LSPR and the magnetic behavior within a composite magnetic/plasmonic material, a feature that we believe to be of great assistance for assessing the response of such hybrid media.

In perspective, we notice that the fabrication procedure reported here for realizing the composite magnetic/plasmonic materials involves the independent synthesis of the magnetic nanocrystals and fabrication of the plasmonic substrate. As such, it easily lends itself to explore novel combinations of magnetic and plasmonic counterparts, whose optical/magnetic response can be independently evaluated and optimized prior to merging them in a single material. The parameters subject to possible optimization are the LSPR wavelength and the MO spectral response, as shown here, but also the LSPR bandwidth or birefringence,[33] and characteristics of the magnetic counterpart, such as the blocking temperature or the coercivity. Furthermore, the self-organization/self-assembly scheme also provides the possibility of fabricating nano objects over large areas, featuring highly homogeneous yet tunable optical, magnetic, and magneto-optical responses, at a low cost.

ASSOCIATED CONTENT

Supporting Information

X-ray absoprtion spectra of the Fe $L_{2,3}$ edge of the iron oxide nanocrystals. MO spectra and hysteresis loops of the Au/LiF and Ag/LiF plasmonic substrates. Description of the fitting procedure for the hysteresis loops. This material is available free of charge via the Internet at http://pubs.acs.org/.

AUTHOR INFORMATION

Corresponding Author

*E-mail: francesco.bisio@spin.cnr.it.

Present Address

[⊥]Laboratory for Micro- and Nanotechnology, Paul Scherrer Institut, 5232 Villigen PSI, Switzerland.

Notes

The authors declare no competing financial interest.

ACKNOWLEDGMENTS

Financial support from the Fondazione Carige, the MIUR (Project No. PRIN 2008AKZSXY_002) and the Università di Genova (PRA 2011) is acknowledged. The authors thank the Colloidal Nanocrystals and Chemistry group at the ICMM/CSIC (Madrid, Spain) for providing the iron-oxide nanocrystals and Ennio Vigo for technical assistance.

REFERENCES

(1) Kreibig, U.; Genzel, L. *Surf. Sci.* **1985**, *156*, 678.
(2) El-Sayed, M. A. *Acc. Chem. Res.* **2001**, *34*, 257.
(3) Kelly, K. L.; Coronado, E.; Zhao, L. L.; Schatz, G. C. *J. Phys. Chem. B* **2003**, *107*, 668.
(4) Jensen, T.; Kelly, L.; Lazarides, A.; Schatz, G. C. *J. Cluster Sci.* **1999**, *10*, 295.
(5) Noguez, C. *J. Phys. Chem. C* **2007**, *111*, 3806.
(6) Shemer, G.; Markovich, G. *J. Phys. Chem. B* **2002**, *106*, 9195.
(7) Li, Y.; Zhang, Q.; Nurmikko, A. V.; Sun, S. *Nano Lett.* **2005**, *5*, 1689.
(8) González-Díaz, J. B.; García-Martín, A.; García-Martín, J. M.; Cebollada, A.; Armelles, G.; Sepúlveda, B.; Alaverdyan, Y.; Köll, M. *Small* **2008**, *4*, 202.
(9) Jain, P. K.; Xiao, Y.; Walsworth, R.; Cohen, A. E. *Nano Lett.* **2009**, *9*, 1644.
(10) Bogani, L.; Cavigli, L.; de Julián Fernández, C.; Mazzoldi, P.; Mattei, G.; Gurioli, M.; Dressel, M.; Gatteschi, D. *Adv. Mater.* **2010**, *22*, 4054.
(11) Wang, L.; Clavero, C.; Huba, Z.; Carroll, K. J.; Carpenter, E. E.; Gu, D.; Lukaszew, R. A. *Nano Lett.* **2011**, *11*, 1237.
(12) Belotelov, V. I.; Akimov, I. A.; Pohl, M.; Kotov, V. A.; Kasture, S.; Vengurlekar, A. S.; Gopal, A. V.; Yakovlev, D. R.; Zvezdin, A. K.; Bayer, M. *Nat. Nanotechnol.* **2011**, *6*, 370.
(13) Tomita, S.; Kato, T.; Tsunashima, S.; Iwata, S.; Fujii, M.; Hayashi, S. *Phys. Rev. Lett.* **2006**, *96*, 167402.
(14) Armelles, G.; González-Díaz, J. B.; García-Martín, A.; García-Martín, J. M.; Cebollada, A.; González, M. U.; Acimovic, S.; Cesario, J.; Quidant, R.; Badenes, G. *Opt. Express* **2008**, *16*, 16104.
(15) Fujikawa, R.; Baryshev, A. V.; Kim, J.; Uchida, H.; Inoue, M. *J. Appl. Phys.* **2008**, *103*, 07D301.
(16) Du, G. X.; Mori, T.; Suzuki, M.; Saito, S.; Fukuda, H.; Takahashi, M. *Appl. Phys. Lett.* **2010**, *96*, 081915.

(17) Challener, W. A.; Peng, C.; Itagi, A. V.; Karns, D.; Peng, W.; Peng, Y.; Yang, X.; Zhu, X.; Gokemeijer, N. J.; Hsia, Y.-T.; Ju, G.; Rottmayer, R. E.; Seigler, M. A.; Gage, E. C. *Nat. Photon.* **2009**, *3*, 220.
(18) Stipe, B. C.; et al. *Nat. Photon.* **2010**, *4*, 484.
(19) Bonanni, V.; Bonetti, S.; Pakizeh, T.; Pirzadeh, Z.; Chen, J.; Nogués, J.; Vavassori, P.; Hillenbrand, R.; Åkerman, J.; Dmitriev, A. *Nano Lett.* **2011**, *11*, 5333.
(20) Valev, V. K.; Silhanek, A. V.; Gillijns, W.; Jeyaram, Y.; Paddubrouskaya, H.; Volodin, A.; Biris, C. G.; Panoiu, N. C.; De Clercq, B.; Ameloot, M.; Aktsipetrov, O. A.; Moshchalkov, V. V.; Verbiest, T. *ACS Nano* **2011**, *5*, 91.
(21) Melle, S.; Menéndez, J. L.; Armelles, G.; Navas, D.; Vázquez, M.; Nielsch, K.; Wehrspohn, R. B.; Gösele, U. *Appl. Phys. Lett.* **2003**, *83*, 4547.
(22) Banthí, J. C.; Meneses-Rodríguez, D.; García, F.; González, M. U.; García-Martín, A.; Cebollada, A.; Armelles, G. *Adv. Mater.* **2012**, *24*, OP36.
(23) González-Díaz, J. B.; Sepúlveda, B.; García-Martín, A.; Armelles, G. *Appl. Phys. Lett.* **2010**, *97*, 043114.
(24) Erskine, J. L.; Stern, E. A. *Phys. Rev. Lett.* **1973**, *30*, 1329.
(25) Višňovský, Š.; Pařízek, V.; Nývlt, M.; Kielar, P.; Prosser, V.; Krishnan, R. *J. Magn. Magn. Mater.* **1993**, *127*, 135.
(26) Wang, L.; Yang, K.; Clavero, C.; Nelson, A. J.; Carroll, K. J.; Carpenter, E. E.; Lukaszew, R. A. *J. Appl. Phys.* **2010**, *107*, 09B303.
(27) Fontijn, W. F. J.; van der Zaag, P. J.; Devillers, M. A. C.; Brabers, V. A. M.; Metselaar, R. *Phys. Rev. B* **1997**, *56*, 5432.
(28) Guerrero, H.; Rosa, G.; Morales, M. P.; del Monte, F.; Moreno, E. M.; Levy, D.; del Real, R. P.; Belenguer, T.; Serna, C. J. *Appl. Phys. Lett.* **1997**, *71*, 2698.
(29) Bentivegna, F.; Nývlt, M.; Ferré, J.; Jamet, J. P.; Brun, A.; Višňovský, S.; Urban, R. *J. Appl. Phys.* **1999**, *85*, 2270.
(30) Kalska, B.; Paggel, J. J.; Fumagalli, P.; Rybczyński, J.; Satula, D.; Hilgendorff, M.; Giersig, M. *J. Appl. Phys.* **2004**, *95*, 1343.
(31) Sugawara, A.; Mae, K. *J. Vac. Sci. Technol. B* **2005**, *23*, 443.
(32) Kitahara, T.; Sugawara, A.; Sano, H.; Mizutani, G. *J. Appl. Phys.* **2004**, *95*, 5002.
(33) Anghinolfi, L.; Moroni, R.; Mattera, L.; Canepa, M.; Bisio, F. *J. Phys. Chem. C* **2011**, *115*, 14036.
(34) Park, J.; An, K.; Hwang, Y.; Park, J.-G.; Noh, H.-J.; Kim, J.-Y.; Park, J.-H.; Hwang, N.-M.; Hyeon, T. *Nat. Mater.* **2004**, *3*, 891.
(35) Salas, G.; Casado, C.; Teran, F. J.; Miranda, R.; Serna, C. J.; Morales, M. P. *J. Mater. Chem.* **2012**, *22*, 21065.
(36) Cabrera, L. I.; Somoza, A.; Marco, J. F.; Serna, C. J.; Morales, M. P. *J. Nanopart. Res.* **2012**, 873.
(37) Anghinolfi, L.; Cabrera, L. I.; Caminale, M.; Moroni, R.; Morales, M. P.; Caprile, L.; Canepa, M.; Mattera, L.; Bisio, F. *Nanosci. Nanotechnol. Lett.* **2012**, *4*, 1087.
(38) Tepper, T.; Ross, C.; Dionne, G. *IEEE Trans. Magn.* **2004**, *40*, 1685.
(39) The actual value for Ag was obtained allowing a slight tarnishing of the sample after its preparation in order to achieve a better matching of the LSPR with the MO response of the iron oxide NCs.
(40) Hui, P. M.; Stroud, D. *Appl. Phys. Lett.* **1987**, *50*, 950.
(41) Sepúlveda, B.; González-Díaz, J. B.; García-Martín, A.; Lechuga, L. M.; Armelles, G. *Phys. Rev. Lett.* **2010**, *104*, 147401.
(42) Du, G. X.; Mori, T.; Saito, S.; Takahashi, M. *Phys. Rev. B* **2010**, *82*, 161403.
(43) Brice-Profeta, S.; Arrio, M.-A.; Tronc, E.; Menguy, N.; Letard, I.; dit Moulin, C. C.; Noguès, M.; Chanéac, C.; Jolivet, J.-P.; Sainctavit, P. *J. Magn. Magn. Mater.* **2005**, *288*, 354.